Contents lists available at **CEPM**

Computational Engineering and Physical Modeling

Journal homepage: www.jcepm.com

Influence of Jeffrey Nanofluid on Peristaltic Motion in an Inclined Endoscope

A.S. Kotnurkar[1*], V.T. Talawar[2]

1. Department of Studies and Research in Mathematics, Karnatak University, Dharwad, 580003, India

Corresponding author: *as.kotnur2008@gmail.com*

https://doi.org/10.22115/CEPM.2021.261607.1142

ARTICLE INFO

Article history:
Received: 11 December 2020
Revised: 11 January 2021
Accepted: 24 April 2021

Keywords:
Peristaltic motion;
Jeffrey nanofluid;
Inclined endoscope;
Homotopy perturbation method.

ABSTRACT

Influence of Jeffrey nanofluid on Peristaltic motion in an Inclined Endoscope where the small intestine, large intestine, or other tracts of the human anatomy are in a cylindrical fashion. Hence in the present paper, we have considered the cylindrical coordinate system. In the gap between two coaxial inclined tubes, we have considered the incompressible non-Newtonian Jeffrey nanofluid. On the assumption of long wavelength and low Reynolds number, the governing equations were investigated. Using the Homotopy Perturbation Technique, coupled equations were solved with the temperature profile and nanoparticle phenomena. Using this present technique, the closed-form solutions of velocity, pressure raise, time-average volume flow rate have been calculated. The important result of this study is that the influence of Jeffrey nanofluid and inclination angle increases the velocity profile. Due to increase in the radius of the inner tube, the velocity of the fluid diminishes. The influence of different physical parameters on temperature, the concentration of nanoparticles, velocity, pressure rise,and frictional force of inner and outer tubes were graphically represented.

How to cite this article: Kotnurkar, A.S., Talawar, V.T. (2021). Influence of Jeffrey Nanofluid on Peristaltic Motion in an Inclined Endoscope. Computational Engineering and Physical Modeling, 4(2), 68–94. https://doi.org/10.22115/cepm.2021.261607.1142

1. Introduction

The Endoscope is an optical illumination system used to get an intense look into the body. An endoscope is a surgical device comprised of a thin, long, and flexible (or rigid) tube that includes a light and video camera at one end to view organs such as the throat or oesophagus, or other parts of the human body. For where they are supposed to look, advanced endoscopes are called, examples include the cystoscope (bladder), gastrointestinal endoscopes, arthroscope (joint), nephroscope (kidney), a laryngoscope (larynx), otoscope (ear), laparoscope (abdomen), and bronchoscope (bronchi). For a medical diagnosis, an endoscope's impact on peristaltic motion is very significant as well as it has many clinical applications. It is an extremely convenient method for identifying actual causes that are responsible for certain complications in human organs where peristaltic pumping transports the fluid. Ramesh and Devakar [1] have discussed the influence of an endoscope on the peristaltic transport of a couple of stress fluid with biomedicine application for heat transfer. Hayat et. al [2] Shahzadi *et al*. [3].

Nomenclature $\frac{dp}{dz}$ pressure gradient

C volumetric volume expansion coefficient ΔP_λ pressure rise

f body forces F_1 frictional force for inner tube

p pressure F_2 frictional force for outer tube

V velocity vector Q time averaged flow rate of volume

k thermal conductivity q volume flow rate

(R, Z) lab frame

Greek letters

$(\tilde{r}, \tilde{z})$ wave frame λ_1 ratio of relaxation to retardation times

(U, W) velocity components in lab frame λ_2 retardation time

$(\tilde{u}, w)$ velocity components inwave frame $\ddot{\gamma}$ differentiation of $\dot{\gamma}$

T nanoparticle temperature ϕ amplitude ratio

C nanoparticle concentration θ dimensionless temperature

D_B Brownian diffusion coefficient δ wave number

$\frac{d}{dt}$ material time derivative σ dimensionless nanoparticle's concentration

D_T thermophoretic diffusion coefficient ρ_f density of fluid

b wave amplitude ρ_p density of particle

a_2 outer tube's radius μ coefficient of viscosity of fluid

a_1 inner tube'sradius λ wavelength

$\tilde{t}$ time β angle of inclination

S Jeffrey fluid's extra stress tensor $\dot{\gamma}$ shear rate

R_e Reynolds number

B_r local concentration Grashof number

N_t thermophoresis parameter

G_r local temperature Grashof number

The concept of peristaltic flow has gained substantial attraction in recent times, due to its growing significance, especially in architecture, science, and biological processes. Due to the several real-life approaches, such as urinary transfer through the ureter from the kidney to the bladder; lymph transfer through the lymphatic vessels; food swallowing through the oesophagus; chyme motion in the gastrointestinal tract; ovum motion in the fallopian tube; Vasomotion of small blood vessels, such as venules, capillaries, and arterioles, as well as the motion of corrosive fluids by sanitary fluids. Since it is considered one of the crucial aspects of transporting fluid in biological processes. The studies reveal that the sinusoidal pressure gradient and motion of the boundaries sustain physiological flows. Latham [4] was the first to introduce Peristalsis in 1966. Shapiro et al. [5] and Jaffrin et al. [6] have further expanded this work. For research, this mechanism has become an essential concept, and many researchers have analyzed both theoretical and practical knowledge of peristaltic flow [7–10].

Most physiological fluids have been recognized to behave as non-Newtonian fluids. Raju and Devanathan [11] were perhaps the first to bring this aspect into consideration. Compared to other fluids, it is one of the simplest fluid models. Study of Jeffrey fluids peristaltic flow useful in physiology and industry owing to its broad number of applications and in mathematics due to its geometry and solutions of non-linear equations. The Jeffrey fluid model, which performs as a Newtonian and non-Newtonian fluid relies on the nub region and perimetric region. Hayat et al. [12], Ebaid et al. [13], Vajravelu et al. [14], Jyothi et al. [15], Akbar et al. [16].

A homogeneous mixture of nanoparticles is known as nanofluid and consists of the elementary fluid. Nanofluid is generally a liquid suspension containing tiny particles between 1 - 100 nm in

diameter. Nanoparticles may be composed of oxides, carbon nanotubes, metals, and carbides. Elementary fluid can include oil, water, and ethylene glycol. Choi [17] was the first who investigated the study on nanoparticles which remarkably raises the thermal conductivity of the elementary fluid. Asha and Sunita [18] investigated the effect of thermal radiation in the presence of gold nanoparticles on the peristaltic blood flow of a Jeffrey fluid with double diffusion. Maruthi et al. [19] the peristaltic transport of a nanofluid was studied in an inclined tube. Noreen Sher Akbar et al. [20] investigated the peristaltic flow of a nanofluid in a non-uniform tube. Akbar and Nadeem [21] analyzed the influence of endoscope on theperistaltic flow of nanofluid. Nadeem et al. [22] focused on the influence of nanoparticles on the peristaltic motion in the annulus of the tangent hyperbolic fluid model. Further, many other researchers have worked on the nanoparticles and influence of the nanoparticle shapes given in the references [23–26].

In the current paper, we have focused influence of Jeffrey Nanofluid on Peristaltic motion in an Inclined Endoscope. The small intestine, large intestine, or other tracts of the human anatomy are in a cylindrical fashion. Hence in the present paper, we have considered the cylindrical coordinate system. In the gap between two coaxial inclined tubes, we have considered the incompressible non-Newtonian Jeffrey nanofluid. The governing equation of continuity, energy, temperature, and concentration of nanofluid are solved on the assumption of long wavelength and low Reynolds number. Using the Homotopy Perturbation Technique, coupled equations were solved with the temperature profile and nanoparticle phenomena. The analytical solutions of velocity, pressure gradient, pressure rise, and frictional force for inner and outer tubes were achieved. The influence of different physical parameters on temperature, the concentration of nanoparticles, velocity, pressure rise,and frictional force of inner and outer tubes were graphically represented at the end of the session.

2. Fundamental equations

Equations for the incompressible fluid for the mass balance, momentum, temperature, and volume fraction of the nanoparticle are given by [27]

$$div V = 0,$$

$$\rho_f \frac{dV}{dt} = -\nabla p + \mu \nabla^2 V + f,$$

$$(\rho C)_f \frac{dT}{dt} = k\nabla^2 T + (\rho C)_p \left[D_B \nabla C.\nabla T + \frac{D_T}{T_0} \nabla T.\nabla T \right],$$

$$\frac{dC}{dt} = D_B \nabla^2 C + \left[\frac{D_T}{T_0} \right] \nabla^2 T,$$

Wherethe context values of T and C as $\tilde{r}$ leads to r_1 and r_2 are denoted by T_0, C_0 and T_1, C_1 respectively.

3. Mathematical formulation:

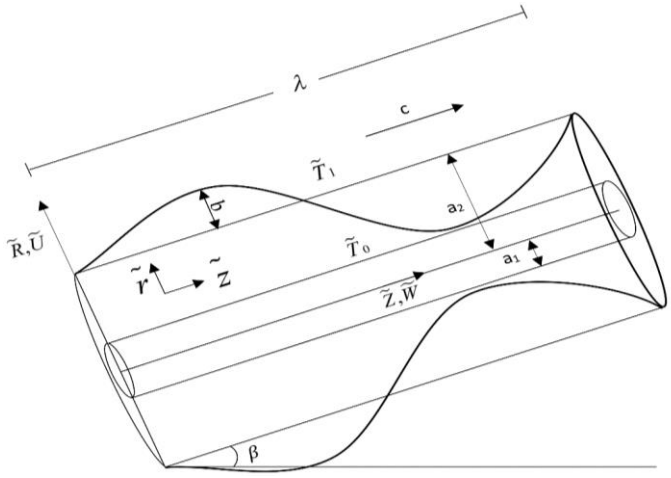

Fig. 1.

Consider the peristaltic flow in an inclined tube with an inserted endoscope of an incompressible non-Newtonian Jeffrey nanofluid. The inner tube is fixed while a sinusoidal wave with velocity c propagates along the outer tube. The flexible characteristics of the inner and outer tubes are also considered. The endoscope and peristaltic tubes are treated as inner and outer concentric tubes. The cylindrical form $\left(R, Z\right)$ has been chosen in that manner Z is considered across the centreline of the tube and R is considered across the radial tendency. The geometry of the inner and outer tubes wall surfaces are given by the equations

$$R_1 = a_1 \tag{1}$$

$$R_2 = a_2 + b\sin\frac{2\pi}{\lambda}\left(\tilde{z} - c\tilde{t}\right) \tag{2}$$

Using the modifications

$$\tilde{z} = Z - c\tilde{t},\ \tilde{r} = R,\ w = W - c,\ u = U \tag{3}$$

The equation for incompressible non-Newtonian Jeffrey nanofluid is given as follows

$$S = \frac{\mu}{1+\lambda_1}\left(\dot{\gamma} + \lambda_2\ddot{\gamma}\right) \tag{4}$$

In an inclined cylindrical coordinate system $\left(R, Z\right)$, the governing equations of the peristaltic transport of an incompressible non-Newtonian Jeffrey fluid are given by

$$\frac{1}{\tilde{r}}\frac{\partial(\tilde{r}u)}{\partial\tilde{r}}+\frac{\partial w}{\partial\tilde{z}}=0 \tag{5}$$

$$\rho\left[u\frac{\partial u}{\partial\tilde{r}}+w\frac{\partial u}{\partial\tilde{z}}\right]=-\frac{\partial p}{\partial\tilde{r}}+\frac{1}{\tilde{r}}\frac{\partial(\tilde{r}S_{\tilde{r}\tilde{r}})}{\partial\tilde{r}}+\frac{\partial S_{\tilde{r}\tilde{z}}}{\partial\tilde{z}}-\frac{S_{\theta\theta}}{\tilde{r}}-\rho g\cos\beta \tag{6}$$

For these two equations the non-dimensional terms are

$$r=\frac{\tilde{r}}{a_2},\quad z=\frac{\tilde{z}}{\lambda},\quad W=\frac{W}{c},\quad R=\frac{R}{a_2}, w=\frac{w}{c},\quad U=\frac{\lambda U}{a_2 c},\quad u=\frac{\lambda u}{a_2 c},\quad Z=\frac{Z}{\lambda},\quad p=\frac{a_2^2 p}{c\lambda\mu}\ \delta=\frac{a_2}{\lambda},$$

$$R_e=\frac{\rho c a_2}{\mu}. \tag{7}$$

$$\begin{aligned}\rho\left[u\frac{\partial w}{\partial\tilde{r}}+w\frac{\partial w}{\partial\tilde{z}}\right]=&-\frac{\partial p}{\partial\tilde{z}}+\frac{1}{\tilde{r}}\frac{\partial(\tilde{r}S_{\tilde{r}\tilde{z}})}{\partial\tilde{r}}+\frac{\partial S_{\tilde{z}\tilde{z}}}{\partial\tilde{z}}\\&+\rho g(T-T_0)+\rho g(C-C_0)+\rho g\sin\beta\end{aligned} \tag{8}$$

For the above equation non-dimensional terms are

$$F=\frac{c\mu}{\rho g a_2^2}, G_r=\frac{\rho g\alpha a_2^2\left(T_0-T_1\right)}{\mu c}, B_r=\frac{\rho g\alpha a_2^2\left(C_0-C_1\right)}{\mu c}. \tag{9}$$

$$\begin{aligned}\left[u\frac{\partial T}{\partial\tilde{r}}+w\frac{\partial T}{\partial\tilde{z}}\right]=&\alpha\left[\frac{\partial^2 T}{\partial\tilde{r}^2}+\frac{1}{\tilde{r}}\frac{\partial T}{\partial\tilde{r}}+\frac{\partial^2 T}{\partial\tilde{z}^2}\right]\\&+\tau\left\{D_B\left[\frac{\partial C}{\partial\tilde{r}}\frac{\partial T}{\partial\tilde{r}}+\frac{\partial C}{\partial\tilde{z}}\frac{\partial T}{\partial\tilde{z}}\right]+\frac{D_T}{T_m}\left[\left(\frac{\partial T}{\partial\tilde{r}}\right)^2+\left(\frac{\partial T}{\partial\tilde{z}}\right)^2\right]\right\}\end{aligned} \tag{10}$$

$$\left[u\frac{\partial C}{\partial\tilde{r}}+w\frac{\partial C}{\partial\tilde{z}}\right]=D_B\left[\frac{\partial^2 C}{\partial\tilde{r}^2}+\frac{1}{\tilde{r}}\frac{\partial C}{\partial\tilde{r}}+\frac{\partial^2 C}{\partial\tilde{z}^2}\right]+\frac{D_T}{T_m}\left[\frac{\partial^2 T}{\partial\tilde{r}^2}+\frac{1}{\tilde{r}}\frac{\partial T}{\partial\tilde{r}}+\frac{\partial^2 T}{\partial\tilde{z}^2}\right] \tag{11}$$

For the above two equations the non-dimensional terms are

$$\theta=\frac{\left(T-T_1\right)}{\left(T_0-T_1\right)},\sigma=\frac{\left(C-C_1\right)}{\left(C_0-C_1\right)},t=\frac{c\tilde{t}}{\lambda},\alpha=\frac{k}{\left(\rho C\right)_f},N_b=\frac{\left(\rho C\right)_p D_B\left(C_0-C_1\right)}{\left(\rho C\right)_f \alpha},$$

$$N_t=\frac{\left(\rho C\right)_p D_T\left(T_0-T_1\right)}{\left(\rho C\right)_f T_m\alpha} \tag{12}$$

Where $\tau=\frac{\left(\rho C\right)_p}{\left(\rho C\right)_f}$ the ratio between the nanoparticle material's effective

heat potential and the fluid's heat capability.

Jeffrey fluid's non-dimensional stress constituents are given as below

$$S_{rr}=\frac{2\delta}{\left(1+\lambda_1\right)}\left(1+\frac{\lambda_2 c\delta}{a}\left(u\frac{\partial}{\partial r}+w\frac{\partial}{\partial z}\right)\right)\frac{\partial u}{\partial r} \tag{13}$$

$$S_{rz}=\frac{1}{\left(1+\lambda_1\right)}\left(1+\frac{\lambda_2 c\delta}{a}\left(u\frac{\partial}{\partial r}+w\frac{\partial}{\partial z}\right)\right)\left(\delta^2\frac{\partial u}{\partial z}+\frac{\partial w}{\partial r}\right) \tag{14}$$

$$S_{\theta\theta}=\frac{2\delta}{\left(1+\lambda_1\right)}\left(1+\frac{\lambda_2 c\delta}{a}\left(u\frac{\partial}{\partial r}+w\frac{\partial}{\partial z}\right)\right)\frac{u}{r} \tag{15}$$

$$S_{zz}=\frac{2\delta}{\left(1+\lambda_1\right)}\left(1+\frac{\lambda_2 \delta c}{a}\left(u\frac{\partial}{\partial r}+w\frac{\partial}{\partial z}\right)\right)\frac{\partial w}{\partial z} \tag{16}$$

In the wave frame, the boundary conditions are as follows

$$w=-c,\ T=T_0,\ C=C_0 \text{ at } \tilde{r}=\tilde{r}_1 \tag{17}$$

$$w=-c,\ T=T_1,\ C=C_1 \text{ at } \tilde{r}=\tilde{r}_2 \tag{18}$$

The dimensionless parameters are given by

$$r_1=\frac{\tilde{r}_1}{a_2}=\frac{a_1}{a_2}=\varepsilon<1\ ,\ \phi=\frac{b}{a_2}<1\ ,\ T=\frac{a_2 T}{c\mu}, \tag{19}$$

Substituting dimensionless parameters into equations (5) to (18) and utilising the assumption of long wavelength and low Reynolds number, after that equations (5) to(18) brings down to the following pattern.

$$\frac{\partial u}{\partial r}+\frac{u}{r}+\frac{\partial w}{\partial z}=0 \tag{20}$$

$$\frac{\partial p}{\partial r}=0 \tag{21}$$

$$\frac{\partial p}{\partial z}=\frac{1}{r\left(1+\lambda_1\right)}\frac{\partial}{\partial r}\left(r\frac{\partial w}{\partial r}\right)+G_r\theta+B_r\sigma+\frac{\sin\beta}{F} \tag{22}$$

$$0=\frac{1}{r}\frac{\partial}{\partial r}\left(r\frac{\partial\theta}{\partial r}\right)+N_b\left(\frac{\partial\sigma}{\partial r}\frac{\partial\theta}{\partial r}\right)+N_t\left(\frac{\partial\theta}{\partial r}\right)^2 \tag{23}$$

$$0=\frac{1}{r}\frac{\partial}{\partial r}\left(r\frac{\partial\sigma}{\partial r}\right)+\frac{N_t}{N_b}\left(\frac{1}{r}\frac{\partial}{\partial r}\left(r\frac{\partial\theta}{\partial r}\right)\right) \tag{24}$$

The appropriate conditions for dimensionless boundaries are given by

$$w=-1,\ \theta=1,\ \sigma=1 \quad \text{at } r=r_1=\varepsilon \tag{25}$$

$$w=-1,\ \theta=0,\ \sigma=0 \quad \text{at } r=r_2=1+\phi\sin 2\pi z \tag{26}$$

3. Analytical determination

The combination of the method of Homotopy and the method of perturbation is considered as the Homotopy perturbation method (HPM) [28–32]. This strategy removes the disadvantages found in the conventional approach of disruption and all the rewards remain the same at the same time. To solve the equations (23) - (24) Homotopy Perturbation Method (HPM) is used.

According to the Homotopy Perturbation Method (HPM), we have to define the equations (23) and (24) as below

$$H\left(m,\theta\right)=\left(1-m\right)\left[L\left(\theta\right)-L\left(\theta_{10}\right)\right]+m\left[L\left(\theta\right)+N_b\left(\frac{\partial\sigma}{\partial r}\frac{\partial\theta}{\partial r}\right)+N_t\left(\frac{\partial\theta}{\partial r}\right)^2\right] \tag{27}$$

$$H\left(m,\sigma\right)=\left(1-m\right)\left[L\left(\sigma\right)-L\left(\sigma_{10}\right)\right]+m\left[L\left(\sigma\right)+\frac{N_t}{N_b}\left(\frac{1}{r}\frac{\partial}{\partial r}\left(r\frac{\partial\theta}{\partial r}\right)\right)\right] \tag{28}$$

Here the linear operator $L=\frac{1}{r}\frac{\partial}{\partial r}\left(r\frac{\partial}{\partial r}\right)$ is considered for our comfort. The initial guesses of the above equation which satisfies the boundary conditions can be defined as

$$\theta_{10} = \frac{\log r - \log r_2}{\log r_1 - \log r_2} = \sigma_{10} \tag{29}$$

Let us define

$$\theta(r,z) = \theta_0 + m\theta_1 + m^2\theta_2 + \text{--------} \tag{30}$$

$$\sigma(r,z) = \sigma_0 + m\sigma_1 + m^2\sigma_2 + \text{------} \tag{31}$$

In most instances the series (30) and (31) are convergent. The convergent frequency, however, relies on the nonlinear aspect of the equation to be calculated.

According to the HPM [28–32] we have obtained the solution for temperature and nanoparticles concentration phenomenon for m=1 as follows

$$\theta(r,z) = \frac{(\log r - \log r_2)}{12A_8^3}[-\frac{A_4}{2}(\log r - \log r_1)(2\log r - A_8) - 6(N_b + N_t)(\log r - \log r_1)A_8 + 12A_8^2] \tag{32}$$

$$\sigma(r,z) = \frac{(\log r - \log r_2)}{12N_bA_8^3}[12N_bA_8^2 + N_tA_4(\log r)(\log r - \log r_1) - N_tA_5(\log r - \log r_1) + N_t(\log r - \log r_1)A_6] \tag{33}$$

Introducing the equations (32) - (33) within the equation (22) and implementing conditions of boundaries the resultant solution for velocity is as follows

$$w = \frac{A_1}{A_8}[\frac{A_2}{4}A_{24} + \frac{A_3}{8}[r^2(A_4A_8A_{25} + A_{26} + A_{27}) - \log r(A_{28} - A_{29} + A_{30}) - 3A_{31} - A_{32} + 2A_4A_{13} - 2A_7A_{14}]] - 1 \tag{34}$$

The dimension less flow rate is provided as

$$q = 2\int_{r_1}^{r_2} rwdr \tag{35}$$

Now introducing the equation (34) into equation (35), the resultant value of the volume flow rate will be

$$q = \left[A_{15}\left[\left(\frac{dp}{dz} - \frac{\sin\beta}{F}\right)A_{16} + A_3(A_{17} + A_{18} + A_{19} - A_{20} + A_{21})\right]\right] - A_{22} \tag{36}$$

By using equation (36), we obtained the value of pressure gradient $\frac{dp}{dz}$ is as follows

$$\frac{dp}{dz} = \frac{1}{A_{16}}\left[\left(\frac{q + A_{22}}{A_{15}}\right) - A_3(A_{17} + A_{18} + A_{19} - A_{20} + A_{21})\right] + \frac{\sin\beta}{F} \tag{37}$$

The pressure rise over a wavelength ΔP_λ and frictional force F on inner tube and outer tube respectively are defined as

$$\Delta P_\lambda = \int_0^1 \frac{dp}{dz} dz \,(38)\, F_1 = \int_0^1 r_1^2 \left(-\frac{dp}{dz} \right) dz \tag{39}$$

$$F_2 = \int_0^1 r_2^2 \left(-\frac{dp}{dz} \right) dz \tag{40}$$

The time averaged flow rate of volume [19], Q is given by

$$Q = q + 1 + \frac{\phi^2}{2} - \varepsilon^2 \tag{41}$$

4. Results and discussions

In the present paper, the analytical determination of the peristaltic motion of Jeffery nanofluid in an inclined endoscope is gained. The analytical results for physical parameters θ, σ, w, q, $\frac{dp}{dz}$, ΔP_λ ,F_1, F_2,and Q are given by the equations (32),(33),(34),(36),(37),(38),(39),(40) and (41) respectively. The numerical solutions of physical parameters are calculated by using MATHEMATICA 11 software and they are graphically represented by using ORIGIN software.Table:1 represents the comparison of velocity profile with open literature. Fig 2(a) - 2(e) represents the pressure (ΔP_λ) versus time-averaged volume flow rate (Q) .Fig 3(a) - 3(e) represents the velocity (w) versus r. Fig 4(a) and 4(b) represents the temperature (θ) versus r. Fig 5(a) and 5(b) represent the concentration (σ) versus r. Figures 6(a) - 6(e) and 7(a) - 7(e) represent the graph of frictional force versus time-averaged volume flow rate (Q) of inner and outer tubes respectively.

As shown in figures 2(a) – 2(e) the impact of different parameters on pressure rise (ΔP_λ), local temperature Grashof number (Gr), a radius of the endoscope (ε), inclination angle (β), local concentration Grashof number (Br), Jeffrey fluid parameter (λ_1). According to these graphs, it is noticed that the pressure decreases as local temperature Grashof number (Gr) increases but it increases as inclination angle (β) and local concentration Grashof number (Br) increases. The pressure rises (0 to 0.55) and decreases (0.56 to 1) as the inner tube radius ε decreases but pressure decreases (0 to 0.1) and increases (0.11 to 1) as Jeffrey fluid parameter λ_1.

In figures 3(a) - 3(e) the graph is plotted for velocity (w) versus r for different values of Gr, Br, β, λ_1, ε . The velocity (w) increases as (β), (λ_1), (Gr) increases but velocity (w) decreases as local concentration Grashof number (Br), inner tube radius (ε) increases.

The figures 4(a) - 4(b) are the graphical representation of temperature (θ) versus r, in these graphs the temperature (θ) increases as Brownian motion parameter N_b and thermophoresis parameter N_t increases. With an increase in Brownian motion and thermophoretic effects, an active movement of nanoparticles from the wall to the fluid occurs, which leads to a significant rise in temperature.

In figures 5(a) - 5(b) the graphical representation of the concentration of nanoparticles (σ) against r, in these graphs, the nanoparticle concentration (σ) increases as Brownian motion parameter N_b increases but (σ) decreases as thermophoresis parameter N_t decreases. Because the heat transfer rate is high in the presence of nanoparticles, it leads to disturbance in the system.

The figures 6(a) - 6(e) and 7(a) - 7(e) represents the graph of frictional force versus time-averaged volume flow rate (Q) of inner and outer tubes (F_1,F_2) respectively, the impact of different parameters such as β, Gr, Br, ε and λ_1 are observed. The frictional force of inner and outer tubes increases as inclination angle (β) increase**.** Frictional force of the inner tube increases as local temperature Grashof number (Gr) increases but the frictional force of the outer tube decreases as (Gr) increases. In the same way, as local concentration Grashof number (Br) increases then inner frictional force F_1decreasesbut outer frictional force F_2 increases. F_1 decreases from 0 to 0.2 and increases from 0.2 to 1 as radius of the inner tube (ε) increases and in the outer tube F_2decreases from 0 to 0.5 and increases from 0.5 to 1 as ε increases. F_1 and F_2 increases from 0 to 0.1 and decreases from 0.1 to 1 as $\lambda_1$increases. These figures demonstrate that F_1 and F_2 have an opposite activity in comparison to the pressure rise(ΔP_λ) against the physical parameters. Furthermore, the frictional force is higher on the outer tube F_2 than the frictional force on the inner tube F_1.

Table 1

Comparison of velocity profile for ε = 0.1, z= 0.5, ϕ = 0.2.

r	**Nadeem et. al** [33]	**Present work**
0.1	-1	-1
0.2	-1.0202	-1.0201
0.3	-1.0301	-1.0294
0.4	-1.0333	-1.0334
0.5	-1.0340	-1.0339
0.6	-1.0321	-1.0315
0.7	-1.0300	-1.0267
0.8	-1.0210	-1.0198
0.9	-1.0107	-1.0108
1	-1	-1

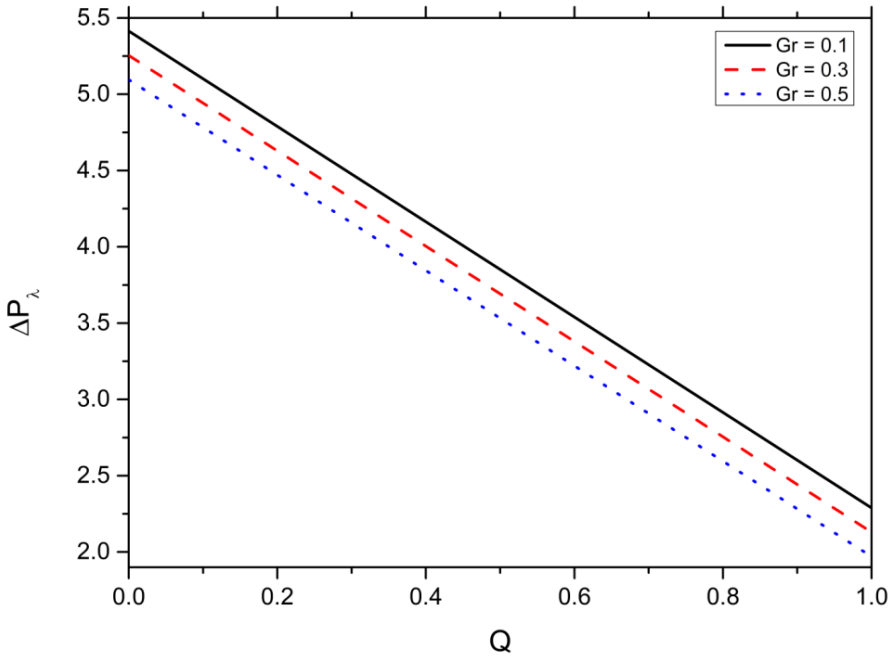

Fig. 2(a). Pressure (ΔP_{λ}) contrary to Q with $N_b = 0.3$, $N_t = 0.4$, $\phi = 0.01$, ε =0.1, Br = 0.3, λ_1 = 0.01, $\beta = \frac{\pi}{6}$, F = 0.1, z = 0.5.

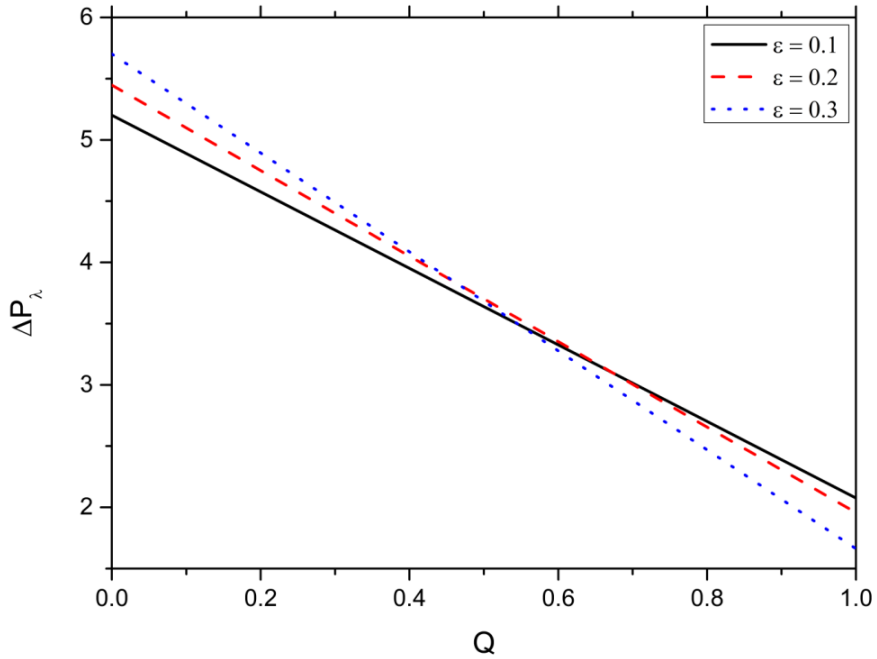

Fig. 2(b). Pressure (ΔP_{λ}) contrary to Q with $N_b = 0.3$, $N_t = 0.4$, $\phi = 0.01$, Gr=0.5, Br = 0.3, $\lambda_1 = 0.01$, $\beta = \frac{\pi}{6}$, F = 0.1, z = 0.5.

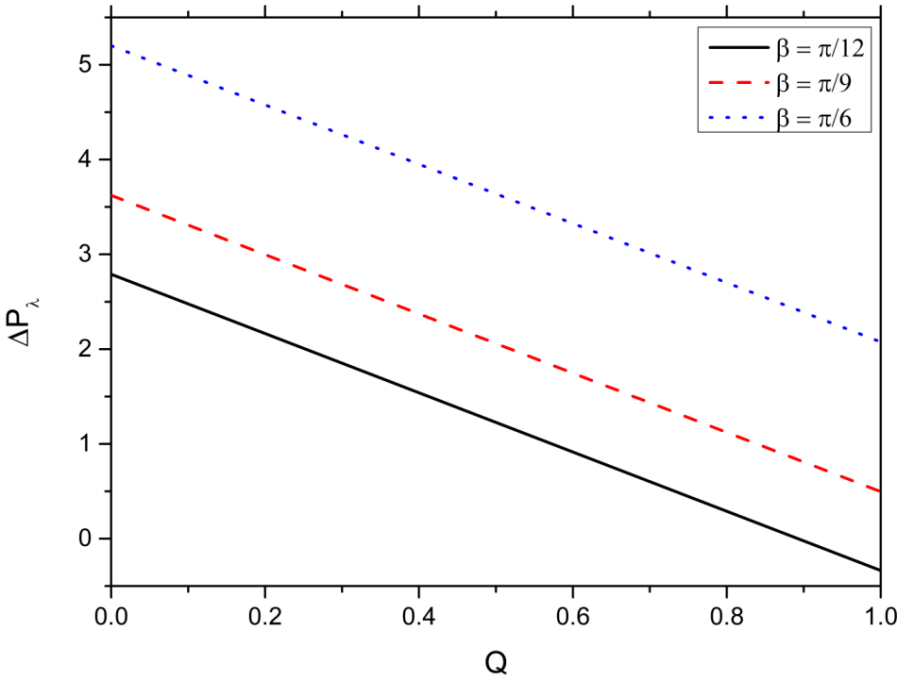

Fig. 2(c). Pressure (ΔP_{λ}) contrary to Q with $N_b = 0.3$, $N_t = 0.4$, $\phi = 0.01$, ε =0.1, Gr = 0.5, z = 0.5, Br = 0.3, $\lambda_1 = 0.01$, F = 0.1.

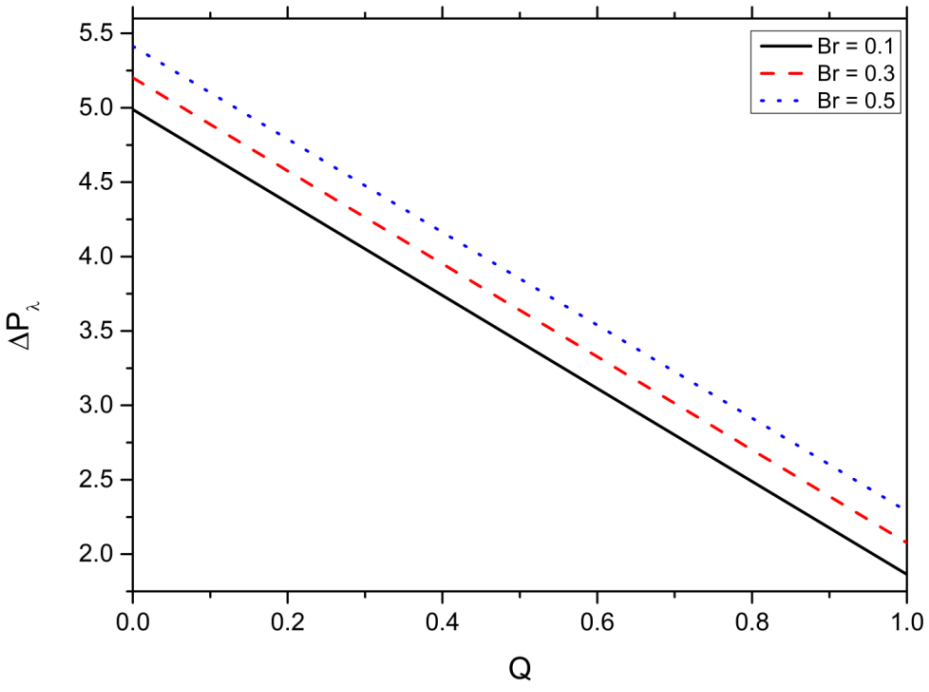

Fig. 2(d). Pressure (ΔP_{λ}) contrary to Q with $N_b = 0.3$, $N_t = 0.4$, $\phi = 0.01$, ε =0.1, Gr = 0.5, $\lambda_1 = 0.01$, $\beta = \frac{\pi}{6}$, F = 0.1, z = 0.5.

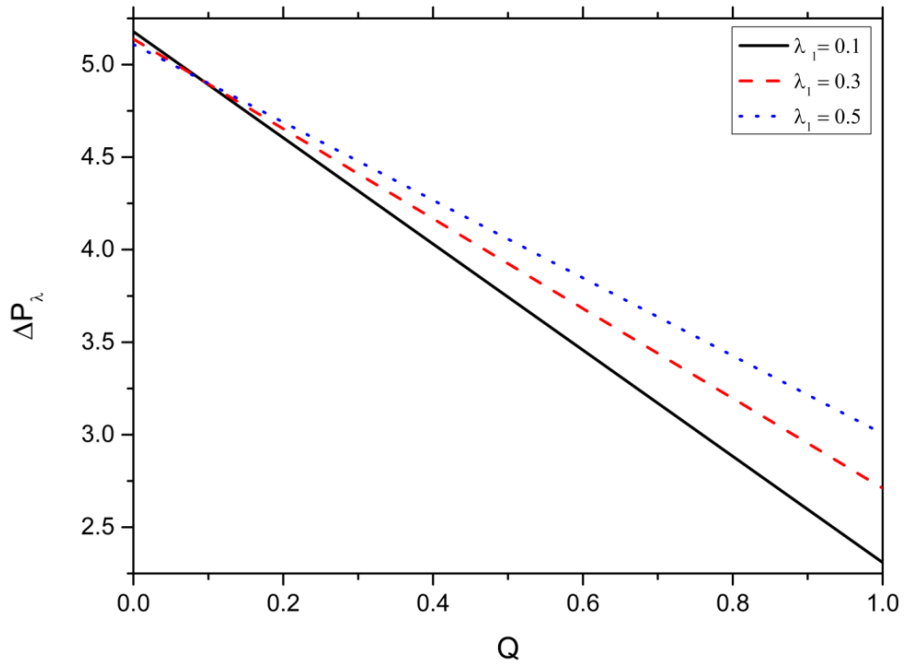

Fig. 2(e). Pressure (ΔP_{λ}) contrary to Q with $N_b = 0.3$, $N_t = 0.4$, $\phi = 0.01$, ε =0.1, Br = 0.3, Gr=0.5, $\beta = \frac{\pi}{6}$, F = 0.1, z = 0.5.

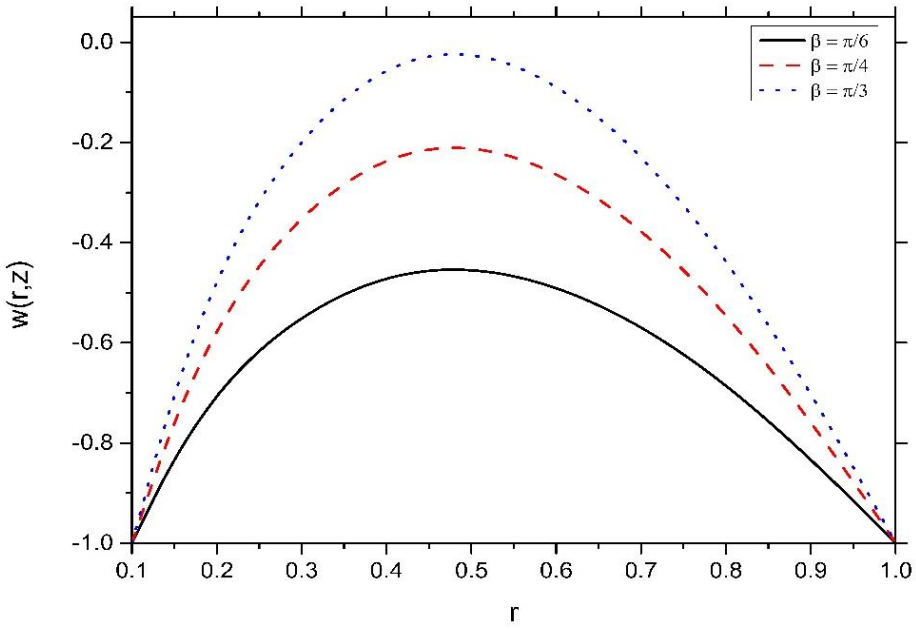

Fig. 3(a). Velocity (w) contrary to r with $\frac{dp}{dz} = 0.4$, $N_b = 0.4$, z = 0.5, $N_t = 0.3$, $\phi = 0.01$, ε =0.1, Gr = 0.5, Br = 0.3, $\lambda_1 = 0.01$, F = 0.1.

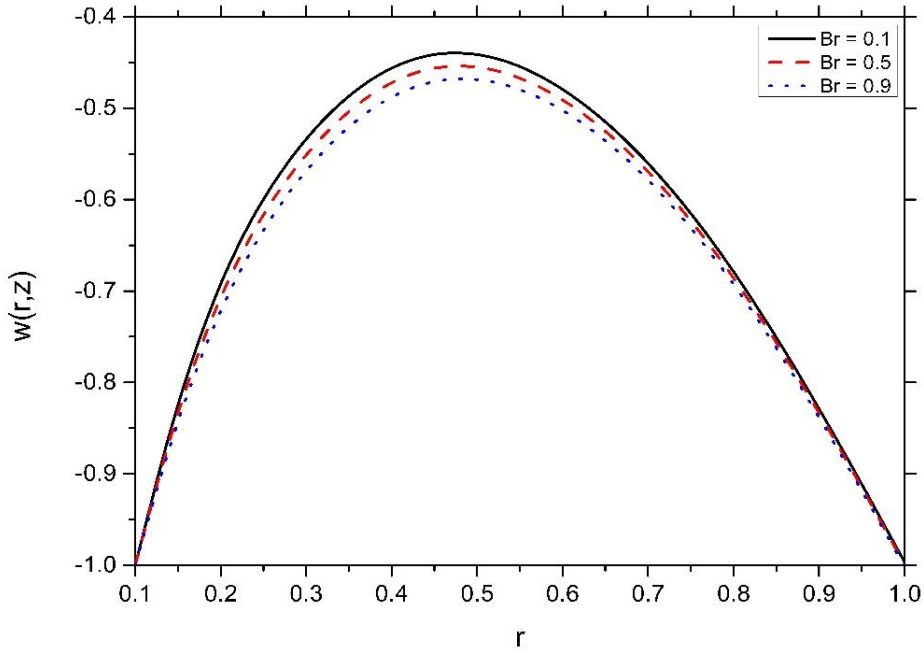

Fig. 3(b). Velocity (w) contrary to r with $N_b = 0.4$, $N_t = 0.3$, $\phi = 0.01$, ε =0.1, Gr = 0.5, Br = 0.3, $\lambda_1 = 0.01$,F = 0.1, $\frac{dp}{dz} = 0.4$, z = 0.5, $\beta = \frac{\pi}{6}$.

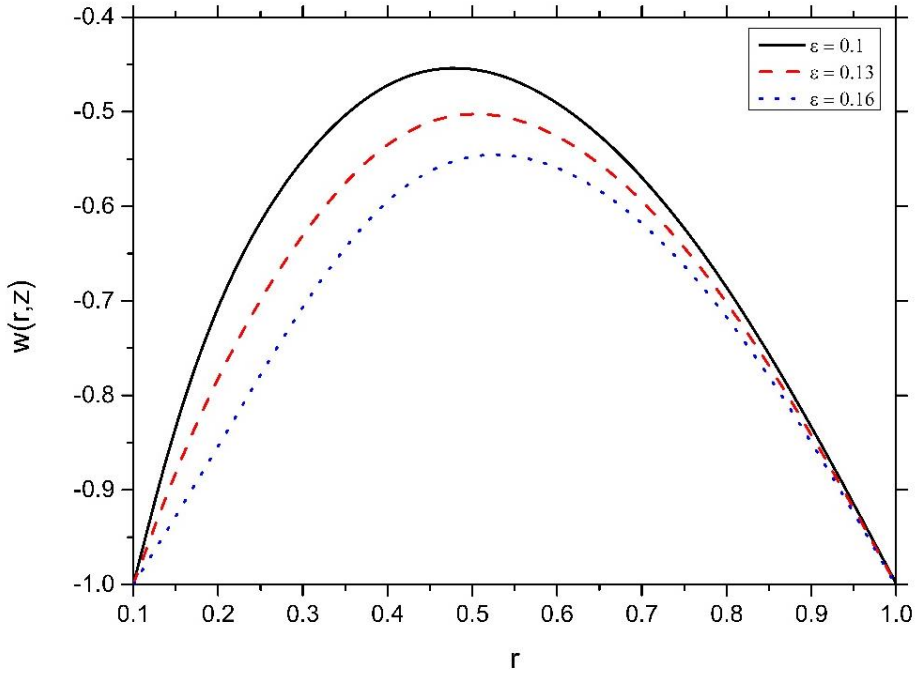

Fig. 3(c). Velocity (w) contrary to r with $N_b = 0.4$, $N_t = 0.3$, $\phi = 0.01$, Gr = 0.5, Br = 0.3, $\lambda_1 = 0.01$, F = 0.1, $\frac{dp}{dz} = 0.4$, z = 0.5, $\beta = \frac{\pi}{6}$.

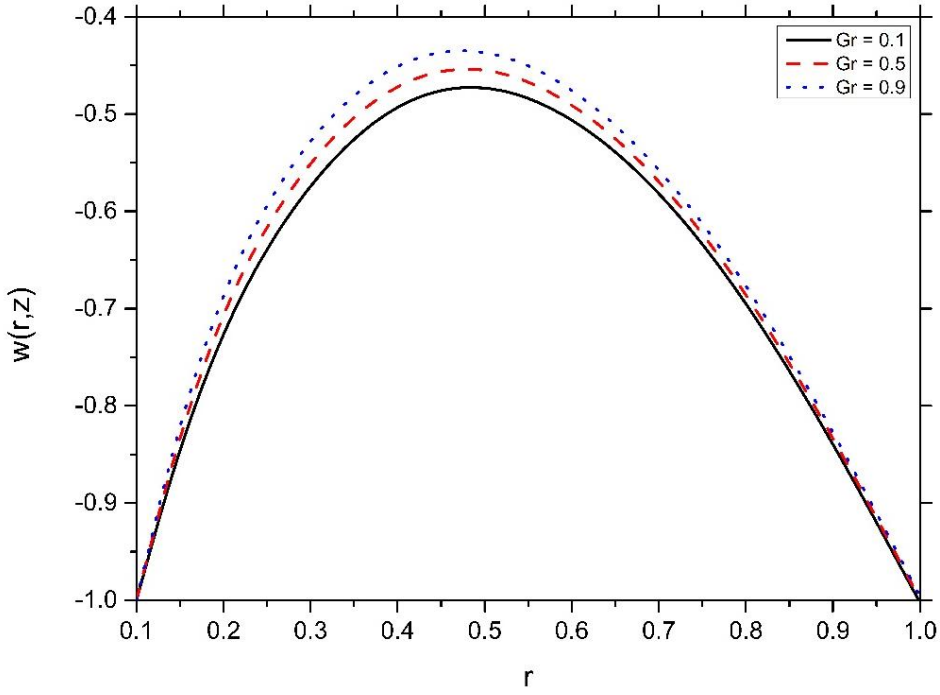

Fig. 3(d): Velocity (w) contrary to r with $N_b = 0.4$, $N_t = 0.3$, $\phi = 0.01$, $\varepsilon = 0.1$, Br = 0.3, $\lambda_1 = 0.01$, F = 0.1, $\frac{dp}{dz} = 0.4$, z = 0.5, $\beta = \frac{\pi}{6}$.

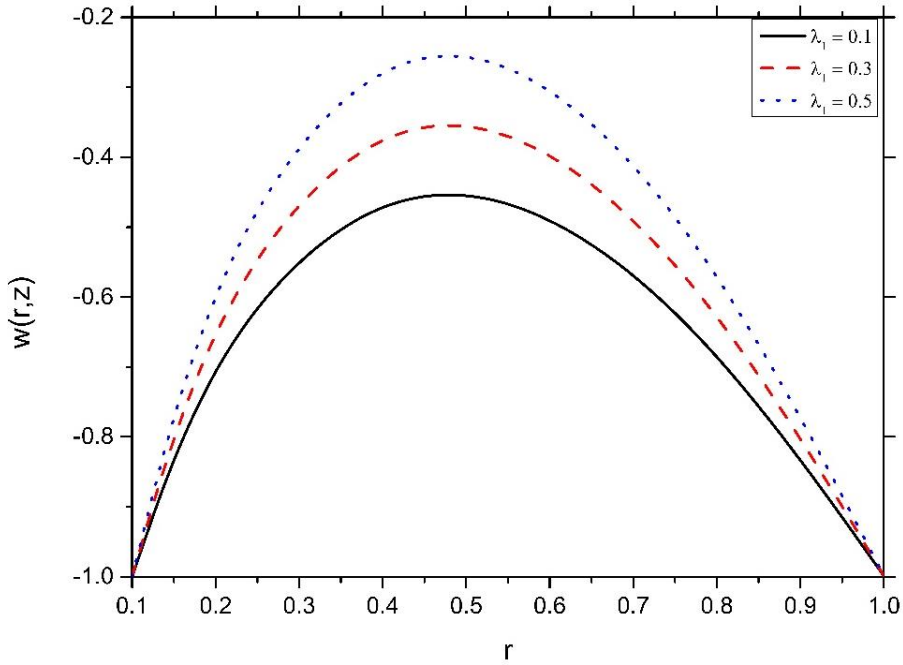

Fig. 3(e). Velocity (w) contrary to r with $N_b = 0.4$, $N_t = 0.3$, $\phi = 0.01$, $\varepsilon = 0.1$, Br = 0.3, F = 0.1, $\frac{dp}{dz} = 0.4$, z = 0.5, $\beta = \frac{\pi}{6}$.

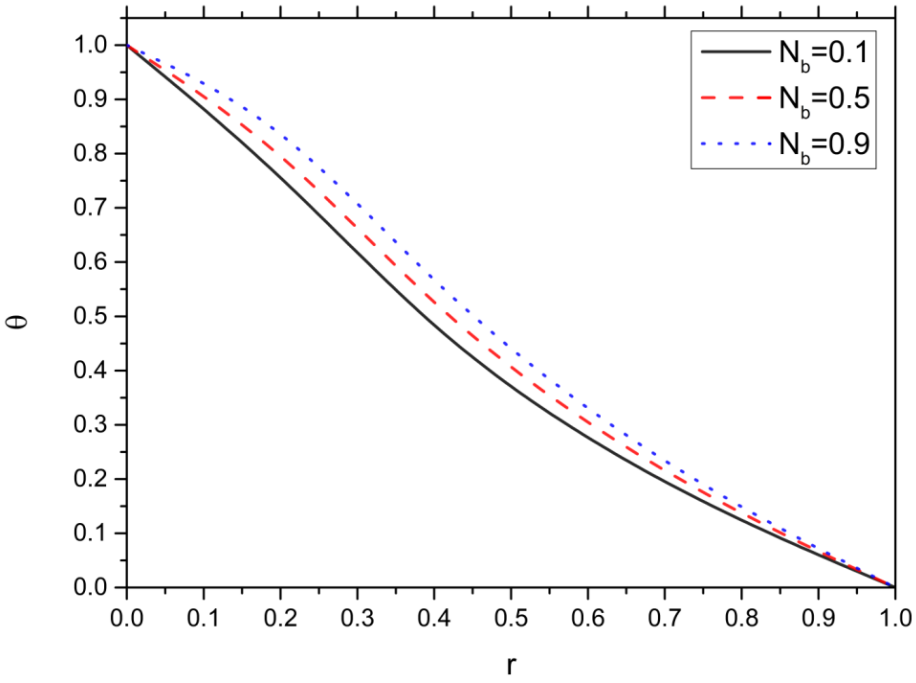

Fig. 4(a). Temperature (θ) contrary to r with $N_t = 0.5$, $\phi = 0.2$, $\varepsilon = 0.1$, z = 0.5.

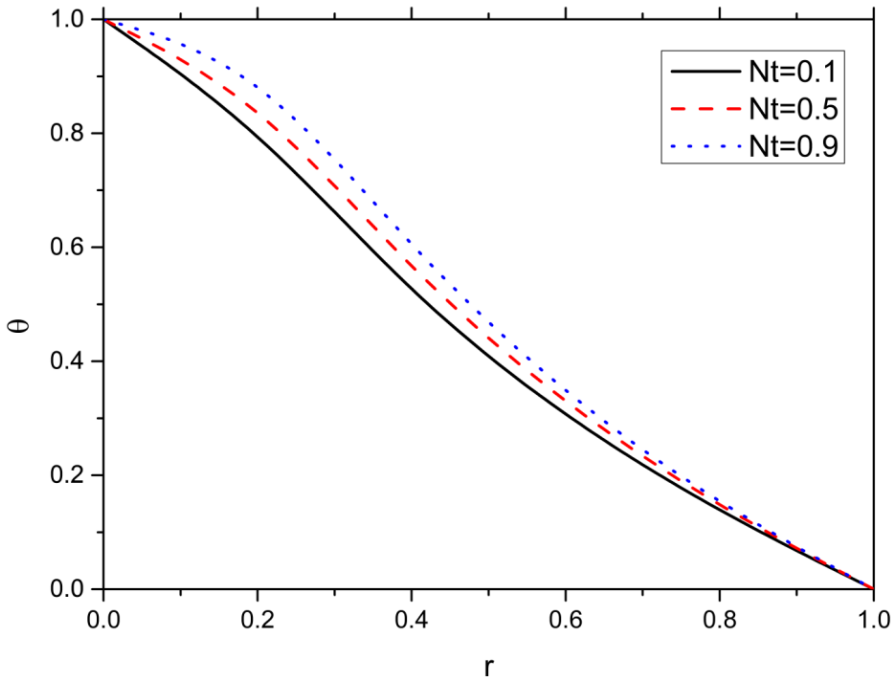

Fig. 4(b). Temperature (θ) contrary to r with $N_b = 0.4$, $\phi = 0.2$, $\varepsilon = 0.1$, z = 0.5.

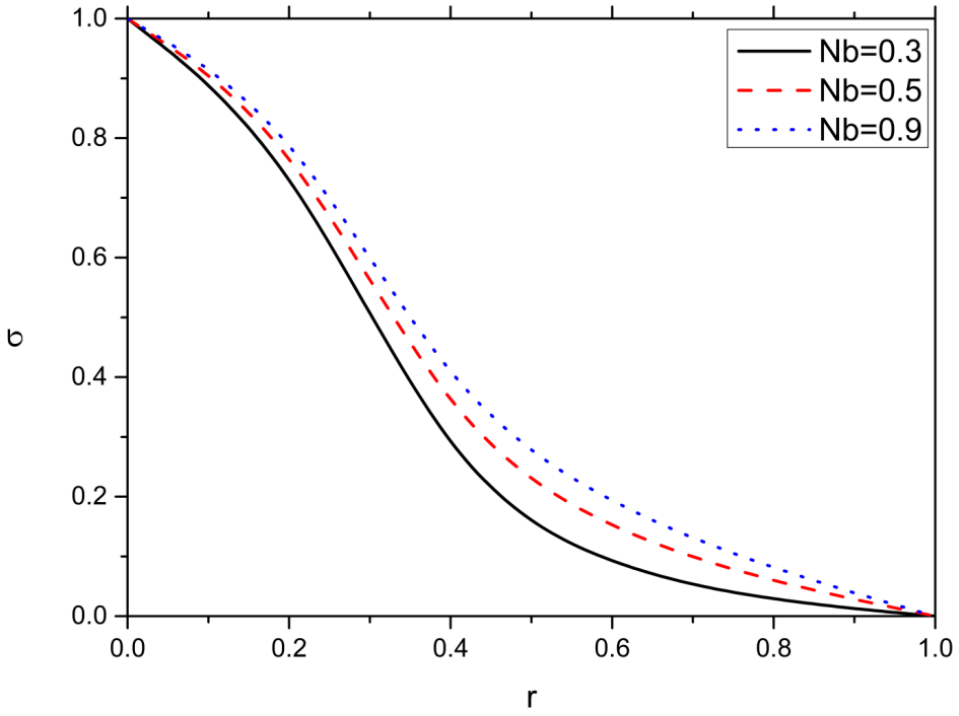

Fig. 5(a). Concentration (σ) contrary to r with ε =0.17, N_t = 0.7, z = 0.5, ϕ = 0.2.

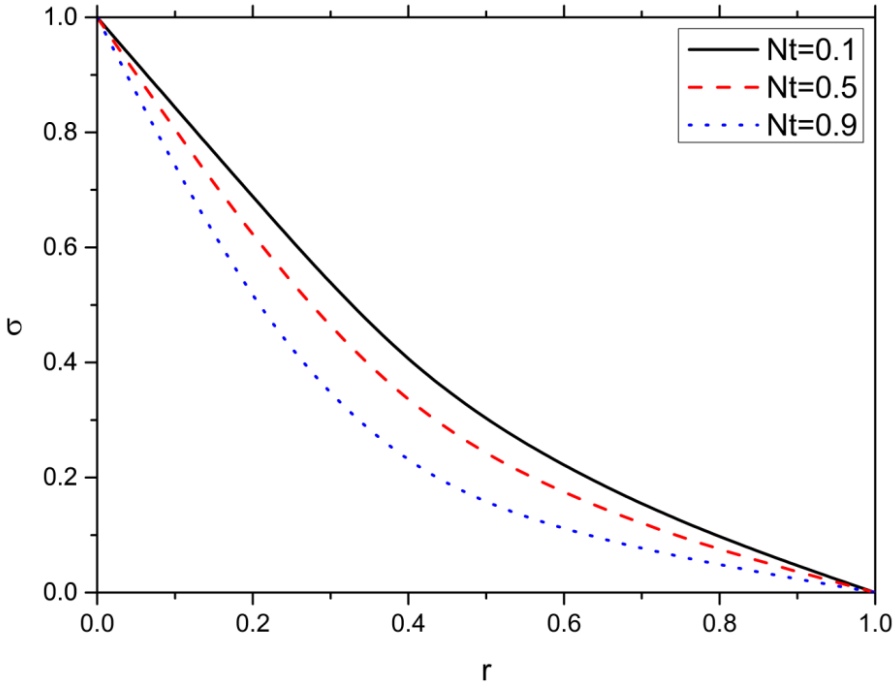

Fig. 5(b). Concentration (σ) contrary to r with N_b = 0.9, ϕ = 0.2, ε =0.1, z = 0.5.

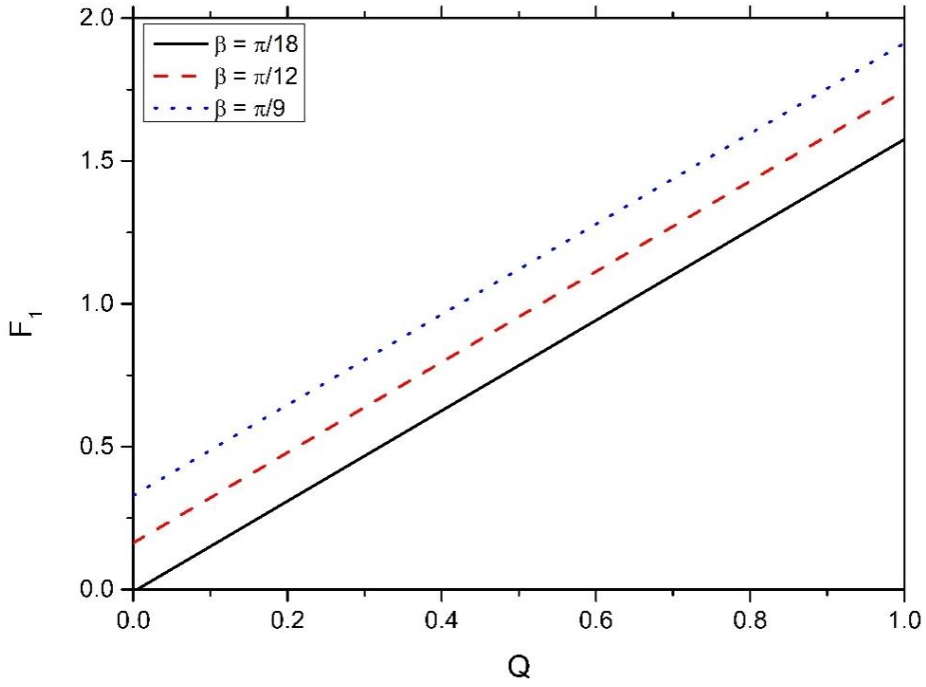

Fig. 6(a). Inner frictional force (F_1) contrary to Q with $N_b = 0.3$, $N_t = 0.4$, $\phi = 0.01$, $\varepsilon = 0.5$, Br = 0.3, Gr=0.5, F = 0.1, z = 0.5, $\lambda_1 = 0.01$.

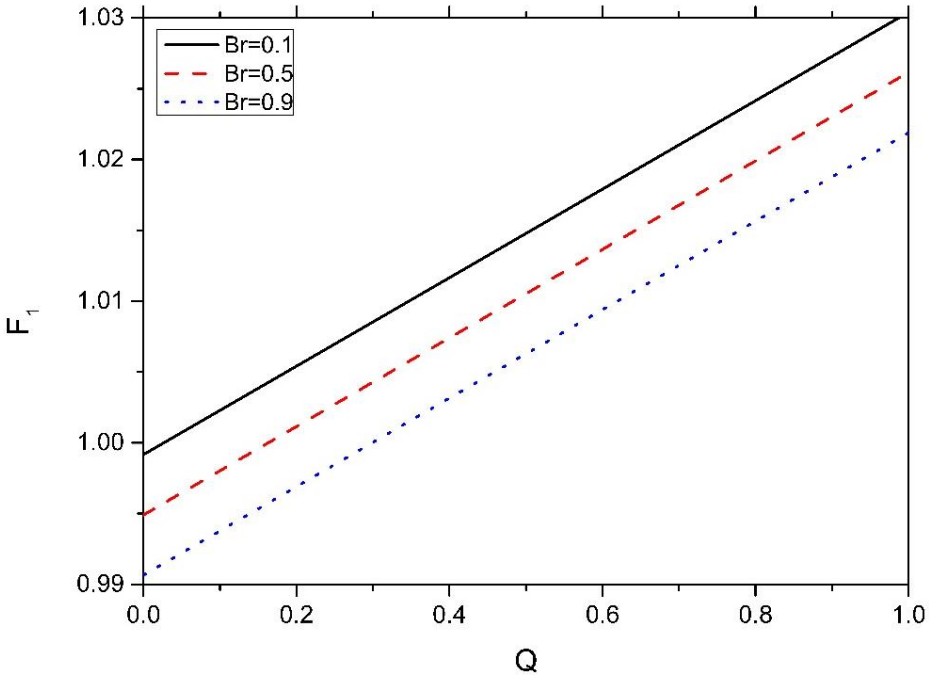

Fig. 6(b). Inner frictional force (F_1) contrary to Q with $N_b = 0.3$, $N_t = 0.4$, $\phi = 0.01$, $\varepsilon = 0.5$, $\beta = \frac{\pi}{6}$, Gr=0.5, F = 0.1, z = 0.5, $\lambda_1 = 0.01$.

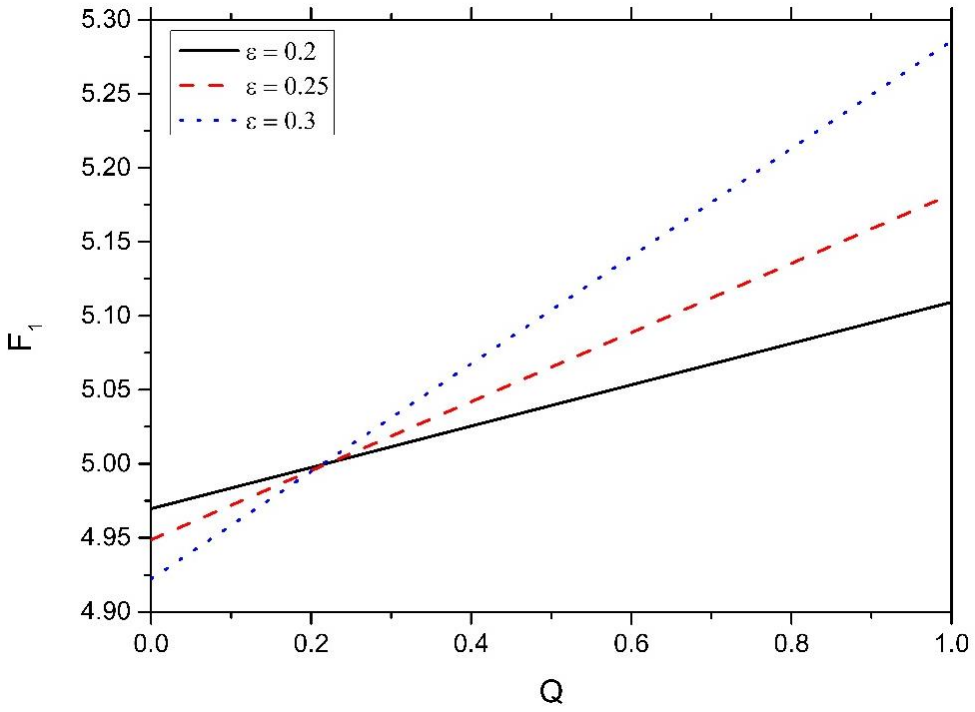

Fig. 6(c). Inner frictional force(F_1) contrary to Q with $N_b = 0.3$, $N_t = 0.4$, $\phi = 0.1$, ε =0.5, Br = 0.3, $\beta = \frac{\pi}{6}$, Gr=0.5, F = 0.1, z = 0.5, $\lambda_1 = 0.01$.

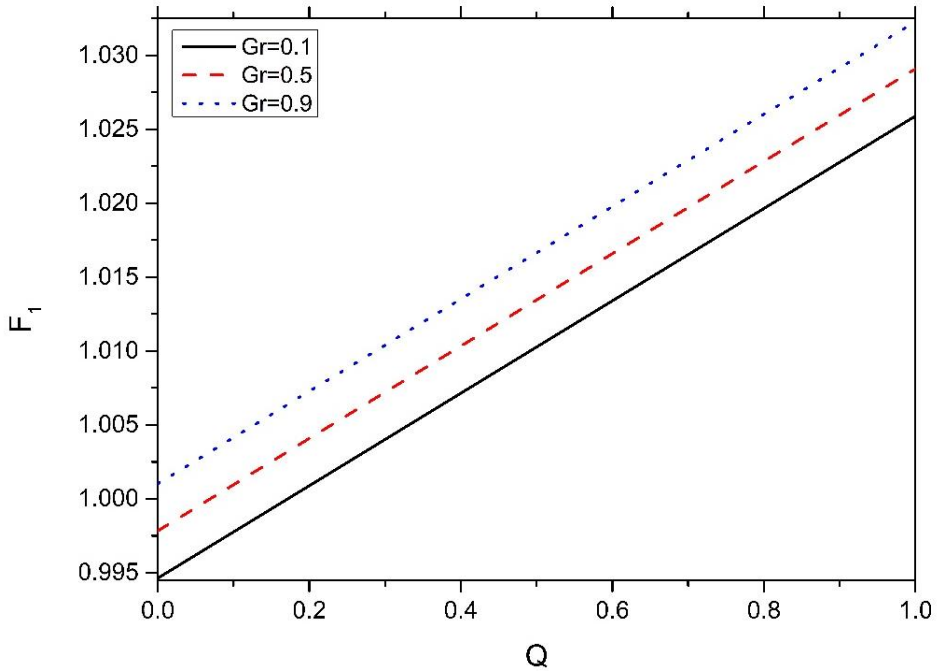

Fig. 6(d). Inner frictional force (F_1) contrary to Q with $N_b = 0.3$, $N_t = 0.4$, ε =0.5, $\phi = 0.01$, Br = 0.3, $\beta = \frac{\pi}{6}$, F = 0.1, z = 0.5, $\lambda_1 = 0.01$.

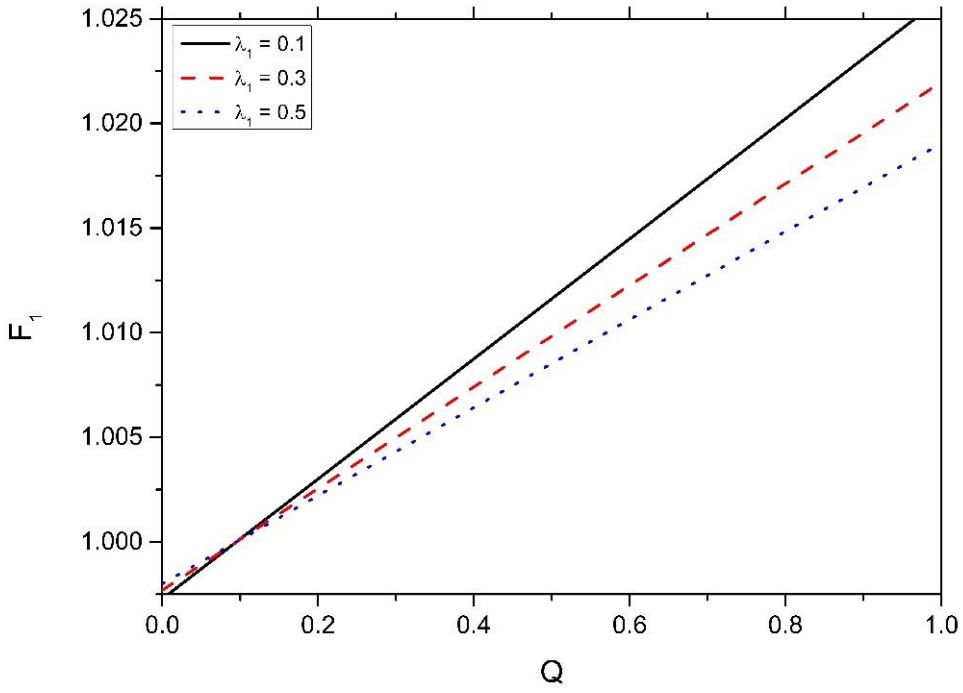

Fig. 6(e). Inner frictional force (F_1) contrary to Q with $N_b = 0.3$, $N_t = 0.4$, $\varepsilon = 0.5$, $\phi = 0.01$, Br = 0.3, $\beta = \frac{\pi}{6}$, F = 0.1, z = 0.5.

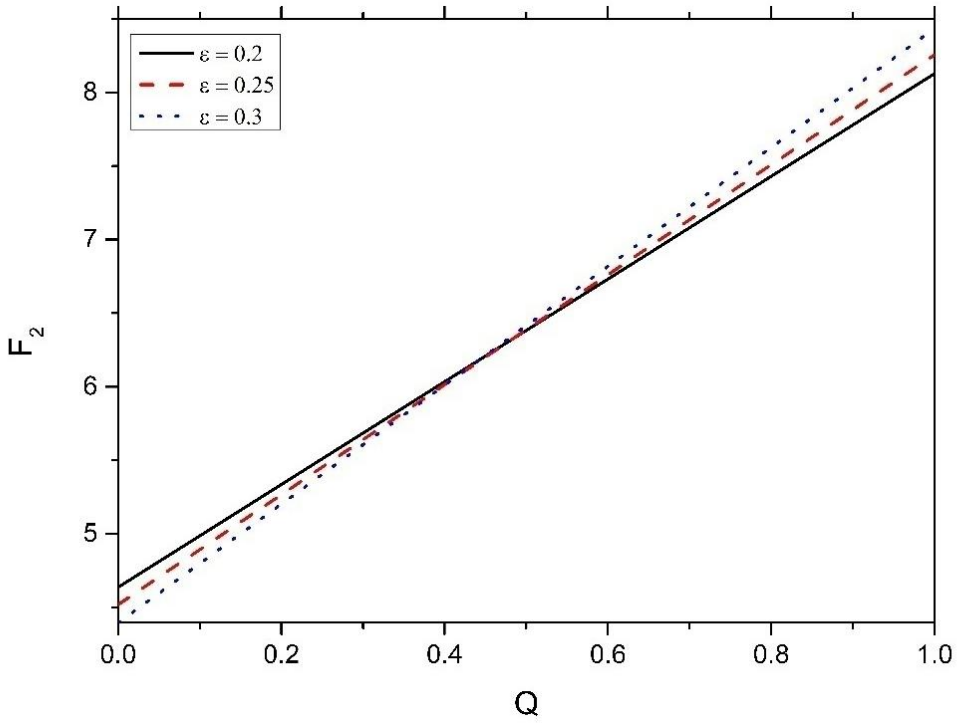

Fig.7 (a). Outer frictional force (F_2) contrary to Q with $N_b = 0.5$, $N_t = 0.1$, $\phi = 0.1$,, Br = 0.2, $\beta = \frac{\pi}{6}$, Gr=0.3, F = 0.1, z = 0.5, $\lambda_1 = 0.01$.

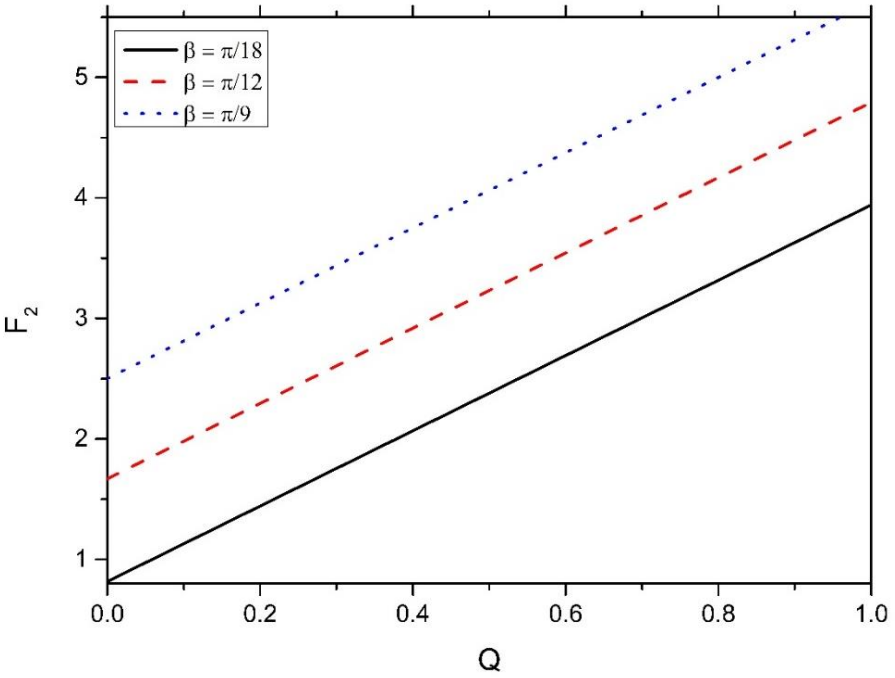

Fig. 7(b). Outer frictional force (F_2) contrary to Q with $N_b = 0.5$, $N_t = 0.1$, $\phi = 0.1$,, Br = 0.2, ε =0.1, Gr=0.3, F = 0.1, z = 0.5, $\lambda_1 = 0.01$.

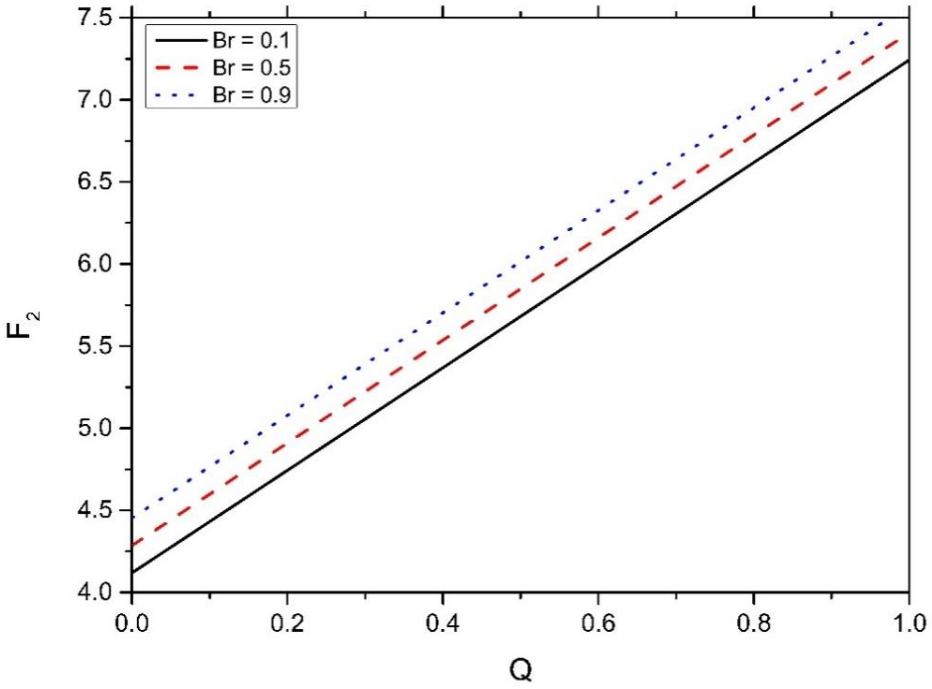

Fig. 7(c). Outer frictional force (F_2) contrary to Q with $N_b = 0.5$, $N_t = 0.1$, $\phi = 0.1$, $\beta = \frac{\pi}{6}$, ε =0.1, Gr=0.3, F = 0.1, z = 0.5, $\lambda_1 = 0.01$.

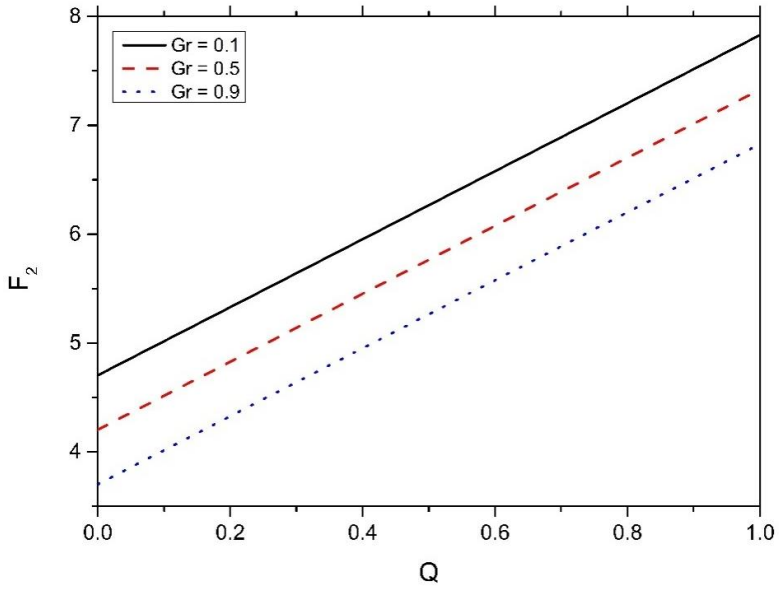

Fig. 7(d). Outer frictional force (F_2) contrary to Q with $N_b = 0.5$, $N_t = 0.1$, $\phi = 0.1$, $\beta = \frac{\pi}{6}$, ε =0.1, Br=0.3, F = 0.1, z = 0.5, $\lambda_1 = 0.01$.

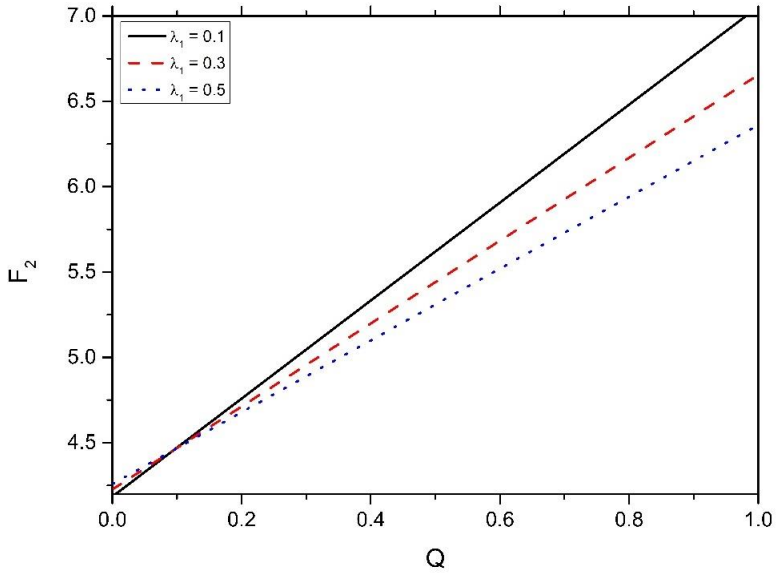

Fig. 7(e). Outer frictional force (F_2) contrary to Q with $N_b = 0.5$, $N_t = 0.1$, $\phi = 0.1$, $\beta = \frac{\pi}{6}$, ε =0.1, Br=0.2, Gr=0.3, F = 0.1, z = 0.5, $\lambda_1 = 0.01$.

5. Conclusion:

This study examines the influence of Jeffrey nanofluid on peristaltic motion in an inclined endoscope under the assumptions of long wave length and low Reynolds number. Temperature profile and nanoparticle phenomena have been calculated using Homotopy Perturbation

Technique while analytical solutions have been calculated for velocity profile, pressure rise, time averaged flow rate and frictional force.

The main points of the current study are as follows:

- Pressure rise (ΔP_λ) increases from 0 to 0.5 and decreases from 0.5 to 1 as radius of the inner tube(ε) increases, it increases as inclination angle(β)increases respectively. Pressure rise (ΔP_λ) decreases from0 to 0.1 and from 0.1 to 1will increase as Jeffrey fluid parameter (λ_1) increases.
- Velocity (w) decreases as radius of inner tube (ε),but velocity increases as inclination angle(β), and Jeffrey fluid parameter (λ_1) increases.
- Temperature profile increases as Brownian motion parameter (Nb) and thermophoresis parameter (Nt) increases.
- Concentration of nanoparticle increases as Brownian motion parameter (Nb) increases but decreases as thermophoresis parameter (Nt) increases.
- Inner frictional force (F_1) and outer frictional force (F_2) both increases as inclination angle (β). $F_1$and F_2 increases from 0 to 0.1 and then decreases from 0.1 to1 as Jeffrey fluid parameter (λ_1) increases.

Acknowledgement

Vijaylaxmi T. Talawar would like to thank Ministry ofTrible Affairs, Government of India for their financial support under NFST scheme [201920-NFST-KAR-02350]Dated:10-4-2020.

Appendix

$$A_1 = \left(1+\lambda_1\right)$$

$$A_2 = \frac{dp}{dz} - \frac{\sin\beta}{F}$$

$$A_3 = \frac{\left(G_r N_b - B_r N_t\right)}{12 N_b \left(\log r_1 - \log r_2\right)^3}$$

$$A_4 = 2\left(N_b + N_t\right)\left(N_b + 2N_t\right)$$

$$A_5 = \left(N_b + N_t\right)\left(N_b + 2N_t\right)\left(\log r_1 - \log r_2\right)$$

$$A_6 = 6\left(N_b + N_t\right)\left(\log r_1 - \log r_2\right)$$

$$A_7 = 12\left(\log r_1 - \log r_2\right)^2\left(\frac{N_b - N_t}{N_t}\right)$$

$$A_8 = \left(\log r_1 - \log r_2\right)$$

$$A_9 = \left(r_1^2 - r_2^2\right)$$

$$A_{10} = r_2^2 \log r_1 - r_1^2 \log r_2$$

$$A_{11} = \left(\left(\log r_1\right)^2 - \left(\log r_2\right)^2\right)$$

$$A_{12} = \left(r_1^2 + r_2^2\right)$$

$$A_{13} = \left(\left(\log r_1\right)\left(\log r_1 - \log r_2\right)\left(r_2^2\left(\log r_1\right) - r_1^2\left(\log r_2\right)\right) + \left(\log r_2\right)\left(\log r_1 - \log r_2\right)\left(r_2^2\left(\log r_2\right) - r_1^2\left(\log r_1\right)\right)\right)$$

$$A_{14} = \left(r_2^2\left(\log r_1\right) - r_1^2\left(\log r_2\right)\right)\left(1 - \log r_1 + \log r_2\right)$$

$$A_{15} = \frac{A_1\left(r_2^2 - r_1^2\right)}{8A_8}$$

$$A_{16} = \left(A_8\left(r_2^2 - r_1^2\right) - 2A_{10} + A_9\left(2\left(\log r_1 - \log r_2\right) + 1\right)\right)$$

$$A_{17} = A_4 A_8 \frac{\left(r_1^2 + r_2^2\right)}{32}\left(-147 - 4\left(\log r_1 + \log r_2\right) + 40\left(\left(\log r_1\right)^2 - \left(\log r_2\right)^2\right) - 128\left(\log r_1 - \log r_2\right)\right)$$

$$A_{18} = \left(A_6 - A_5\right) A_8 \frac{\left(r_1^2 + r_2^2\right)}{8}\left(17 + 20\left(\log r_1 - \log r_2\right)\right)$$

$$A_{19} = A_7 A_8 \frac{\left(r_1^2 + r_2^2\right)}{4}\left(5 + 2\left(\log r_1 - \log r_2\right)\right)$$

$$A_{20} = \left(\left(\log r_1 - \log r_2\right) + \frac{1}{2}\right) A_9\left(2A_4 A_{11} + 6A_4 - 3\left(A_6 - A_5\right) - 2A_7 - 9A_4 A_8 + 4A_8\left(A_6 - A_5\right) + 2A_7 A_8\right)$$

$$A_{21} = \left(2A_4\left(A_{13} - A_7\right) - 3A_{10}\left(A_6 - A_5 - 2A_4\right) - A_{11}\left(2A_9\left(A_6 - A_5\right) - 3A_{12}A_4\right)\right)$$

$$A_{22} = \left(r_2 - r_1\right)$$

$$A_{23} = \left(r_2^2 \log r_1 - r_1^2 \log r_2\right)$$

$$A_{24} = r^2 A_8 - A_9 \log r - A_{10}$$

$$A_{25} = \begin{pmatrix} -6 + 2\left(\log r\right)\left(\log r - \log r_1\right)\left(\log r - \log r_2\right) - 2\left(\log r\right)\left(\log r - \log r_1\right) - 2\left(\log r\right)\left(\log r - \log r_2\right) \\ -2\left(\log r - \log r_1\right)\left(\log r - \log r_2\right) + 3\left(\log r - \log r_1\right) + 3\left(\log r - \log r_2\right) + 3\left(\log r\right) \end{pmatrix}$$

$$A_{26} = \left(A_6 - A_5\right) A_8\left(3 - 2\left(\log r - \log r_1\right) - 2\left(\log r - \log r_2\right) + 2\left(\log r - \log r_1\right)\left(\log r - \log r_2\right)\right)$$

$$A_{27} = A_7 A_8\left(2 - 2\left(\log r - \log r_2\right)\right)$$

$$A_{28} = A_9\left(-6A_4 + 3\left(A_6 - A_5\right) + 2A_7\right)$$

$$A_{29} = 2A_4A_9A_{11}$$

$$A_{30} = A_8A_9\left(9A_4 - 4\left(A_6 - A_5\right) - 2A_7\right)$$

$$A_{31} = A_{23}\left(A_6 - A_5 - 2A_4\right)$$

$$A_{32} = A_{11}\left(2A_9\left(A_6 - A_5\right) - 3A_{12}A_4\right)$$

References

[1] Ramesh K, Devakar M. Effect of endoscope on the peristaltic transport of a couple stress fluid with heat transfer: Application to biomedicine. Nonlinear Eng 2019;8:619–29.

[2] Hayat T, Saleem A, Tanveer A, Alsaadi F. Numerical study for MHD peristaltic flow of Williamson nanofluid in an endoscope with partial slip and wall properties. Int J Heat Mass Transf 2017;114:1181–7. doi:10.1016/j.ijheatmasstransfer.2017.06.066.

[3] Shahzadi I, Nadeem S, Rabiei F. Simultaneous effects of single wall carbon nanotube and effective variable viscosity for peristaltic flow through annulus having permeable walls. Results Phys 2017;7:667–76. doi:10.1016/j.rinp.2016.12.024.

[4] Latham TW. Fluid motions in a peristaltic pump 1966.

[5] Shapiro AH, Jaffrin MY, Weinberg SL. Peristaltic pumping with long wavelengths at low Reynolds number. J Fluid Mech 1969;37:799–825. doi:10.1017/S0022112069000899.

[6] M.Y. J, A.H. S. Peristaltic pumping. Annu Rev Fluid 1971;3:13–36.

[7] Hayat T, Rafiq M, Ahmad B. Soret and Dufour effects on MHD peristaltic flow of Jeffrey fluid in a rotating system with porous medium. PLoS One 2016;11:e0145525.

[8] Asha SK, Sunita G. Effect of couple stress in peristaltic transport of blood flow by homotopy analysis method. AJST 2017;12:6958–64.

[9] Asha SK, Sunitha G. Mixed convection peristaltic flow of a Eyring–Powell nanofluid with magnetic field in a non-uniform channel. JAMS 2018;2:332–4.

[10] Asha SK, Sunitha G. Peristaltic transport of Eyring-Powell nanofluid in a non-uniform channel. Jordan J Math Stat 2019;12:431–53.

[11] Raju KK, Devanathan R. Peristaltic motion of a non-Newtonian fluid. Rheol Acta 1972;11:170–8.

[12] Hayat T, Ali N, Asghar S. An analysis of peristaltic transport for flow of a Jeffrey fluid. Acta Mech 2007;193:101–12. doi:10.1007/s00707-007-0468-2.

[13] Elshehawey EF, Eldabe NT, Elghazy EM, Ebaid A. Peristaltic transport in an asymmetric channel through a porous medium. Appl Math Comput 2006;182:140–50. doi:10.1016/j.amc.2006.03.040.

[14] Vajravelu K, Sreenadh S, Lakshminarayana P. The influence of heat transfer on peristaltic transport of a Jeffrey fluid in a vertical porous stratum. Commun Nonlinear Sci Numer Simul 2011;16:3107–25. doi:10.1016/j.cnsns.2010.11.001.

[15] Jyothi KL, Devaki P, Sreenadh S. Pulsatile flow of a Jeffrey fluid in a circular tube having internal porous lining. Int J Math Arch 2013;4:75–82.

[16] Akbar NS, Nadeem S, Lee C. Characteristics of Jeffrey fluid model for peristaltic flow of chyme in small intestine with magnetic field. Results Phys 2013;3:152–60. doi:10.1016/j.rinp.2013.08.006.

[17] Choi SUS, Eastman JA. Enhancing thermal conductivity of fluids with nanoparticles. Argonne National Lab., IL (United States); 1995.

[18] K AS, G S. Influence of thermal radiation on peristaltic blood flow of a Jeffrey fluid with double

diffusion in the presence of gold nanoparticles. Informatics Med Unlocked 2019;17:100272. doi:10.1016/j.imu.2019.100272.

[19] Prasad KM, Subadra N, Srinivas MAS. Peristaltic transport of a nanofluid in an inclined tube. Am J Comput Appl Math 2015;5:117–28.

[20] Akbar NS, Nadeem S, Hayat T, Hendi AA. Peristaltic flow of a nanofluid in a non-uniform tube. Heat Mass Transf 2012;48:451–9. doi:10.1007/s00231-011-0892-7.

[21] Akbar NS, Nadeem S. Endoscopic effects on peristaltic flow of a nanofluid. Commun Theor Phys 2011;56:761.

[22] Nadeem S, Sadaf H, Akbar NS. Effects of nanoparticles on the peristaltic motion of tangent hyperbolic fluid model in an annulus. Alexandria Eng J 2015;54:843–51. doi:10.1016/j.aej.2015.07.003.

[23] Hosseinzadeh K, Asadi A, Mogharrebi AR, Ermia Azari M, Ganji DD. Investigation of mixture fluid suspended by hybrid nanoparticles over vertical cylinder by considering shape factor effect. J Therm Anal Calorim 2021;143:1081–95. doi:10.1007/s10973-020-09347-x.

[24] Rostami AK, Hosseinzadeh K, Ganji DD. Hydrothermal analysis of ethylene glycol nanofluid in a porous enclosure with complex snowflake shaped inner wall. Waves in Random and Complex Media 2020:1–18. doi:10.1080/17455030.2020.1758358.

[25] Hosseinzadeh K, Roghani S, Asadi A, Mogharrebi A, Ganji DD. Investigation of micropolar hybrid ferrofluid flow over a vertical plate by considering various base fluid and nanoparticle shape factor. Int J Numer Methods Heat Fluid Flow 2020;31:402–17. doi:10.1108/HFF-02-2020-0095.

[26] Hosseinzadeh K, Moghaddam MAE, Asadi A, Mogharrebi AR, Ganji DD. Effect of internal fins along with Hybrid Nano-Particles on solid process in star shape triplex Latent Heat Thermal Energy Storage System by numerical simulation. Renew Energy 2020;154:497–507. doi:10.1016/j.renene.2020.03.054.

[27] Kuznetsov AV, Nield DA. Natural convective boundary-layer flow of a nanofluid past a vertical plate. Int J Therm Sci 2010;49:243–7. doi:10.1016/j.ijthermalsci.2009.07.015.

[28] Akbar NS, Nadeem S, Hayat T, Hendi AA. Peristaltic flow of a nanofluid with slip effects. Meccanica 2012;47:1283–94. doi:10.1007/s11012-011-9512-3.

[29] He J-H. Homotopy perturbation method for solving boundary value problems. Phys Lett A 2006;350:87–8. doi:10.1016/j.physleta.2005.10.005.

[30] He J-H. Application of homotopy perturbation method to nonlinear wave equations. Chaos, Solitons & Fractals 2005;26:695–700. doi:10.1016/j.chaos.2005.03.006.

[31] He J-H. Approximate analytical solution for seepage flow with fractional derivatives in porous media. Comput Methods Appl Mech Eng 1998;167:57–68. doi:10.1016/S0045-7825(98)00108-X.

[32] Soltanian F, Dehghan M, Karbassi SM. Solution of the differential algebraic equations via homotopy perturbation method and their engineering applications. Int J Comput Math 2010;87:1950–74. doi:10.1080/00207160802545908.

[33] Nadeem S, Akbar NS, Hayat T, Hendi AA. Peristaltic flow of Walter's B fluid in endoscope. Appl Math Mech 2011;32:689–700. doi:10.1007/s10483-011-1449-7.